Materials Science and Engineering B 197 (2015) 36–42

Contents lists available at ScienceDirect

Materials Science and Engineering B

journal homepage: www.elsevier.com/locate/mseb

Dielectric-ferrite film heterostructures for magnetic field controlled resonance microwave components

I.V. Zavislyak[a,1], M.A. Popov[a,1], E.D. Solovyova[b,*], S.A. Solopan[b,2], A.G. Belous[b,2]

[a] Faculty of Radiophysics, Electronics and Computer Systems, Taras Shevchenko National University of Kyiv, Kyiv 01601, Ukraine
[b] Department of Solid State Chemistry, V.I. Vernadskii Institute of General and Inorganic Chemistry, 32/34 Prospect Palladina, Kyiv-142, 03680, Ukraine

ARTICLE INFO

Article history:
Received 29 December 2014
Received in revised form 6 March 2015
Accepted 17 March 2015
Available online 30 March 2015

Keywords:
Barium hexaferrite
Nickel ferrite spinel
Thick films
Heterostructures
Microwave resonance components

ABSTRACT

An investigation of the composite "α-Al_2O_3 dielectric resonator-thick ferrite film" heterostructures magnetic field tunable microwave properties has been conducted. Thick high-density high-quality $NiFe_2O_4$ spinel and M-type hexaferrite $BaFe_{12}O_{19}$ films were deposited on the surface of the dielectric by tape-casting technique. Specific organic suspensions for ferrite films synthesis were developed; optimal conditions for pre-heat treatment and annealing have been defined. It was found, that magnetic field has a profound impact on microwave transmission characteristic of composite resonator, including peak absorption level and unloaded *Q*-factor. Both effects were attributed to increase of the magnetic part of the composite resonator internal losses at frequencies close to ferromagnetic resonance. Since qualitatively similar results were obtained for both cm-wave (with nickel ferrite) and mm-wave (with barium hexaferrite) resonators, the proposed method of electronic control over dielectric resonator properties can be successfully utilized in a very broad frequency range, basically, from few GHz to more than 100 GHz.

1. Introduction

Current trends in mobile communications, wireless technologies, satellite television and radiolocation require improvement of the existing UHF components and advancement into new frequency bands [1–3]. Stripline and dielectric resonator based UHF filters are the key elements of the modern transceiver equipment [4–8]. Besides indisputable advantages of such devices (like high quality factor and temperature stability), the lack of dynamical tuning of their characteristics (such as operating frequency, *Q*-factor, insertion losses, etc.) is their crucial drawback, since utilization of electronically tunable components can greatly increase the functionality of microwave devices. Thus, development of tunable devices on the basis of high-*Q* dielectric resonators (DR) is an important and urgent task.

In general, electronic control could be realized if device includes ferroelectric [9], semiconductor [10] or ferrite [11] constituent. This is, in essence, the practical realization of the composite materials concept. In such structures tuning is fulfilled due to the either electric field dependence of added component dielectric constant, conductance and/or capacitance or, as in the last case, due to its high frequency magnetic permeability adjustment with magnetic field. Other tuning techniques, with the assistance of electromechanical actuators, MEMS [10,12] or DR temperature change [13] are also known.

In the first two of abovementioned cases, an undesirable degradation of resonator quality factor and thermostability usually take place, therefore incorporation of ferrite component with tunable permeability seems more advantageous since it allows for purely electronic control over composite resonator electrodynamics characteristics without noticeable deterioration of the *Q*-factor.

In the present paper, we considered the electronic control of RF properties of composite heterostructure, comprising of polycrystalline α-Al_2O_3 bulk DR with a layer of ferrimagnetic material. While tuning mechanism is similar with that, utilized in [11], we exploited thick-film tape-casting ferrite component instead of a bulk ferrite, which, as expected, should decrease mass and dimensions of composite structure, and also make it compatible with planar technology. Large area of contact between ferrite and dielectric in such heterostructure favors substantial penetration of DR main mode high-frequency electromagnetic field into magnetic film, resulting in noticeable impact of ferrite permeability on the

* Corresponding author. Tel.: +380 44 424 22 11; fax: +380 44 424 22 11.
E-mail addresses: zav@univ.kiev.ua (I.V. Zavislyak), maxim_popov@univ.kiev.ua (M.A. Popov), solovyovak@mail.ru (E.D. Solovyova), solopan@ukr.net (S.A. Solopan), belous@ionc.kiev.ua (A.G. Belous).
[1] Tel.: +380 44 521 32 37.
[2] Tel.: +380 44 424 22 11; fax: +380 44 424 22 11.

http://dx.doi.org/10.1016/j.mseb.2015.03.008
0921-5107/

DR resonance mode even for marginal relative volume of the ferrite component. At the same time, small ferrite volume could not lead to substantial degradation of DR eigen-oscillations *Q*-factor, providing that the bias magnetic field is far from resonant value. Such resonators with electronically controlled electrodynamic characteristics can find application in reconfigurable matched filters [14] with dynamic modification of the filter pulse response characteristic in accordance to the spectrum of incoming signal [15]. Besides, as it was demonstrated earlier, two-layered ferrite-dielectric structures can operate as a magnetic field tunable mm-wave band isolator [16].

For the ferrite constituent of composite resonator we selected such traditional microwave ferrites as $NiFe_2O_4$ with spinel structure and M-type barium hexaferrite ($BaFe_{12}O_{19}$). The former is widely used in lower part of microwave frequencies, whereas the latter one (due to the large magnetocrystalline uniaxial anisotropy field) is utilized in millimeter wavelengths, at frequencies above 50 GHz. Hence, this choice of materials allowed us to investigate the suggested composite resonator design in a very broad frequency range.

It is known [17], that in order to get a desired parameters of ferrite microwave devices, a relatively thick film (from few tenths to few hundreds microns) must be utilized. One of the promising techniques for thick crystalline films deposition is a tape-casting [18,19]. It allows to obtain a high-density film and provides capability for film thickness variation during the deposition.

For the manufacturing of a two-layer "α-Al_2O_3 dielectric resonator-ferrite film" structures the film should have high density and homogeneity [20]. The suspension for the thick films deposition by tape-casting method consists of two main components: an inorganic powder precursor and an organic component. Therefore, the production of thick high-density films by tape-casting method is primarily dependent on both the microstructure of the powder precursor (particle size and agglomeration) and the nature of organic components. Also, an important key point during the synthesis of uniform thick films is its annealing conditions (prebaking and final annealing temperatures). Therefore, the development of the main suspension components (powder precursor and organic component) and determination of annealing conditions are important.

The aim of this work is to develop the high-density high-quality nickel ferrite spinel $NiFe_2O_4$ and M-type barium hexaferrite $BaFe_{12}O_{19}$ thick films on the surface of the α-Al_2O_3 bulk dielectric resonator and to produce electronically tunable microwave resonance components for cm- to mm-wave frequency bands on the basis of these two-layer composite structures.

2. Experimental part

2.1. Synthesis of powder precursors

The starting powder precursors for the synthesis of spinel $NiFe_2O_4$ thick films were obtained by the precipitation from non-aqueous solutions according to the method described in [21]. $Fe(NO_3)_3{\cdot}6H_2O$, $Ni(NO_3)_2{\cdot}9H_2O$ (analytical grade), NaOH (purity 97%), diethylene glycol (DEG, purity 99%) and oleic acid (pure OLA) were used as initial reagents. Nanoparticles of $NiFe_2O_4$ were obtained by the heat treatment of prepared solution in the temperature range 200–220 °C (60 h).

The starting powder precursors for the synthesis of M-type barium hexaferrite (BHF) thick films were obtained by the sequential precipitation of barium carbonate on pre-precipitated iron (III) hydroxide from aqueous solutions of their salts in the stochiometric ratio corresponding to the formula $BaFe_{12}O_{19}$. A 1 M solutions of an analytically pure $Fe(NO_3)_3$ and $BaCl_2$ were used. Iron hydroxide was precipitated from an aqueous ammonia solution (pH 4.3) and barium carbonate with an ammonia-carbonate (pH 9) precipitant. Nanoparticles of BHF were obtained by the heat treatment of precipitates at T = 1000 °C. This method of M-type BHF nanoparticles synthesis was described in details in [22].

Samples were investigated by X-ray phase analysis (XPA) and full-profile X-ray phase analysis on a DRON-4 diffractometer (Cu Kα radiation). The size of powder particles was estimated from the broadening of the XRD peaks. Assuming the Gaussian shape of the diffraction peak, the linear line broadening β was calculated from the formula: $\beta = \sqrt{B^2 - b^2}$, where B is the total linear broadening of the line and b is the instrumental broadening. The particles size was calculated from the Scherrer formula: $D = 0.9\lambda/(\beta_{hkl}\cos\theta_{hkl})$. The size and morphology of powder particles have been determined using a SELMI transmission electron microscope (TEM)—125 K at 100 kV of accelerating voltage. Size distribution was obtained from the analysis of TEM images with the use of image tool 3 and Originpro 8.5 Sr1 software packages. When calculating particles size distribution, tem images were analyzed according to the procedure described by Peddis et al. [23].

2.2. Synthesis of spinel $NiFe_2O_4$ and M-type $BaFe_{12}O_{19}$ nanocrystalline thick films

The suspension for film deposition consists of the powder precursor and the organic component. The organic component was a mixture of plasticizer (dibutyl phthalate), dispersant, binder (polymethyl methacrylate, PMMA) and solvents (isopropanol and acetylacetone). Dibutyl phosphate and a mixture of dibutyl phosphate and tannin were used as dispersants. The suspension consists of the precursor powder, isopropanol, dibutyl phosphate, acetylacetone, PMMA and dibutyl phthalate in the ratio of 30%, 22%, 4%, 30%, 9% and 5% of the total weight of suspension component, respectively. The prepared suspension was stirred in a planetary mill (mixing speed 300 rpm, 4 cycles for 30 min).

Thermogravimetric and differential thermal analysis (TGA/DTA) of the obtained suspensions were carried out. The experiments were conducted in dynamic air or oxygen atmospheres, 100 mL/min, in the T = 20–1000 °C temperature range, using a SDT Q600 V8.1 Build 99 equipment.

Then, the obtained suspensions were deposited by the type-casting method (DEPOSITION RATE WAS 0.1 MM/S) on α-Al_2O_3 dielectric resonators.

The prebaking of the thick films was carried out at slow heating and thermal shock conditions at 500 °C, using a heating rate of 30 °C/min. The films underwent final annealing in a conventional furnace at a heating rate of 60 °C/h. Temperature ranges were T = 800–1100 °C and T = 1000–1300 °C for $NiFe_2O_4$ and M-type $BaFe_{12}O_{19}$ thick films, respectively.

Synthesized films were characterized by X-ray diffraction analysis (XRD) on X'pert powder PAN Analytical diffractometer with Cu Kα radiation and Bragg–Brentano geometry. For the phase characterization, the JCPDS database was used.

The micrographs of the films were obtained using field emission gun scanning electron microscope (JSM 6510LV, Jeol, Japan).

2.3. Transmission characteristics of the composite "α-Al_2O_3-thick ferrite film" resonators

2.3.1. Composite resonator "α-Al_2O_3-nickel ferrite"

Investigation of the composite dielectric-ferrite resonator properties in centimeter wave band were conducted using custom made measuring cell. The cell was comprised from a microstrip transmission line section, placed inside a shielding metallic case. The microstrip transmission line was manufactured from a 0.01-in.

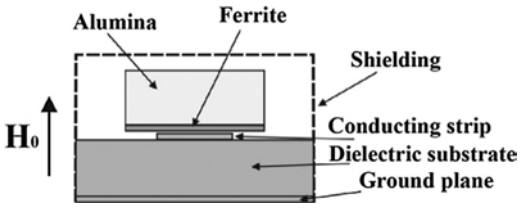

Fig. 1. Cross-section of the shielded microstrip transmission line with heterostructure under study.

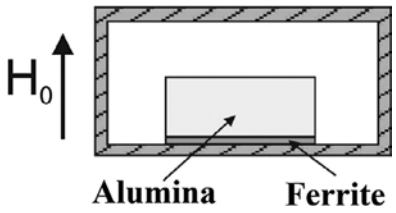

Fig. 2. Cross-section of the V-band rectangular waveguide with composite resonator inside.

thick RT Duroid 5880 substrate ($\varepsilon_r = 2.2$). The conductor strip width was 0.75 mm and the impedance of the transmission line was equal to 50 Ω. SMA-type connectors were used on both sides of the measuring cell. An empty waveguide section was tested in advance and insertion losses were found to be 0.75–1 db in 10–11 GHz frequency range, whereas standing wave ratio (SWR) was less than 2.

During the measurements, composite resonator was put atop of the microstrip, such that ferrite film was in direct contact with metal stripe. External bias magnetic field was created by permanent magnet and pointed perpendicularly to the sample surface (see Fig. 1). Measurements were done using Agilent N5230A vector network analyzer. Before the measurements a two-port TRM (thru, reflect, match) calibration was performed. Since a complete shielding of measuring cell was provided, resonator radiation losses were excluded and a narrow resonance linewidth was obtained with loaded *Q*-factor determined only by material tg δ and coupling losses.

Measurements were done in a traveling wave mode, since in such way an effective excitation of both dielectric resonance in alumina DR and ferromagnetic resonance (FMR) in ferrite were assured. As soon as RF magnetic field in the film region has an almost linear polarization in the direction perpendicular to both waveguide axis [8] and magnetic field, an optimal conditions for FMR excitation were provided. Absorption spectra of composite structure were recorder at few fixed values of magnetic field, with frequency scanned from 1 to 20 GHz.

Lateral dimensions of the rectangular α-Al_2O_3 resonator were 8 and 12 mm and thickness was 3 mm. Our calculations for the given DR dimensions, assuming $\varepsilon = 9.8$ and taking into account top and bottom metal surfaces lead to the lowest mode frequency equal to $F_{H_{01\delta}} = 11.06$ GHz, that is rather close to the experimentally observed value. Nickel ferrite film thickness was estimated to be 30 μm.

From the measured transmission characteristic an unloaded Q-factor value was extracted, using a well-known technique [4], considering resonator as a local inhomogeneity in a terminated transmission line. Thus, we calculated $Q_0 = 940 \pm 40$ for heterostructure without magnetic field, dropping to minimum $Q_0 = 526 \pm 13$ when FMR frequency coincides with $F_{H_{01\delta}}$.

2.3.2. Composite resonator "α-Al2O3–barium hexaferrite"

Since FMR frequency in M-type hexaferrites belongs to mm-wave band [24], interaction between ferromagnetic and dielectric resonances under perpendicular bias is possible only at frequencies, exceeding the natural domain resonance frequency (approximately 47 GHz for pure barium hexaferrite). Hence, in this case the composite resonator was placed inside a metal rectangular V-band waveguide (with 1.8 mm × 3.6 mm cross-section). An appropriately smaller alumina resonator (length 3.4 mm, width 2.0 mm, thickness 1 mm) was fabricated, to ensure that lower order dielectric modes frequencies would fit into abovementioned frequency band. Thickness of the tape-casting deposited barium hexaferrite film was 50 μm. Sample was positioned at the middle of the waveguide wide wall. Magnetic field was created by electromagnet and directed along the normal to the sample surface (Fig. 2).

Transmission characteristics of heterostructure were observed with scalar network analyzer P2-69 and then recorded into PC using custom-made ADC circuitry. Before the measurements an empty waveguide calibration was used, and thus waveguide insertion losses were effectively cancelled out.

3. Results and discussion

3.1. Nickel ferrite spinel $NiFe_2O_4$

The single-phase nanoparticles which are characterized by nanosize weakly-agglomerated particles ($D_{AV.} = 5$ nm) and a narrow size distribution with 95% of the particles having the size of 3–6 nm were used as powder precursor for the synthesis of $NiFe_2O_4$ thick films (Fig. 3). Particles sizes obtained from results of SEM are consistent with the particles sizes, calculated from the broadening of X-ray reflections.

The organic component of the suspension for the films synthesis was a mixture of plasticizer, dispersant, binder and solvents. The dispersant is one of the most important ingredients. It prevents particles adhesion in the solution, increases the suspension stability [25,26] and contributes to obtaining high density thick films [25,27]. According to the literature, dibutyl phosphate is the most widely used dispersant for the synthesis of thick films by tape-casting method. However, films obtained in such way are often characterized by a porous structure [25]. Also, there are reports [28] that tannin can enhance the suspension stability and, correspondingly, the thick film density. Therefore in this study, dibutyl phosphate and a mixture of dibutyl phosphate and tannin were used as dispersants.

Thermal decomposition process of the film-form solution was studied for defining the temperature range of the organic component elimination from the suspension and, therefore, the prebaking temperatures of the films (Fig. 4). As follows from Fig. 4, the DTA

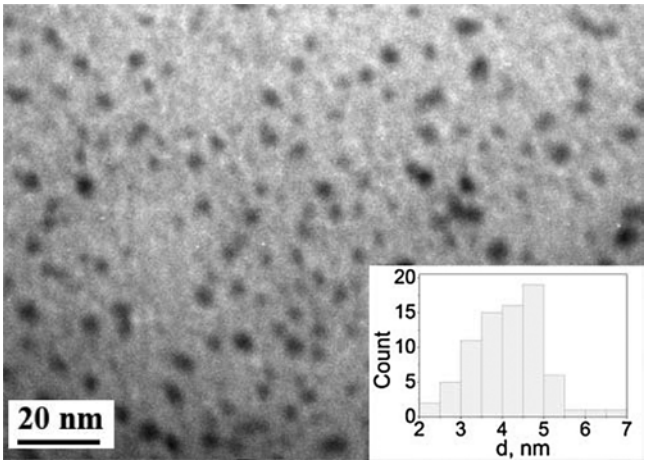

Fig. 3. The microstructure of $NiFe_2O_4$ nanoparticles, obtained at $T = 220$ °C. Insets: size distribution diagram for $NiFe_2O_4$ nanoparticles.

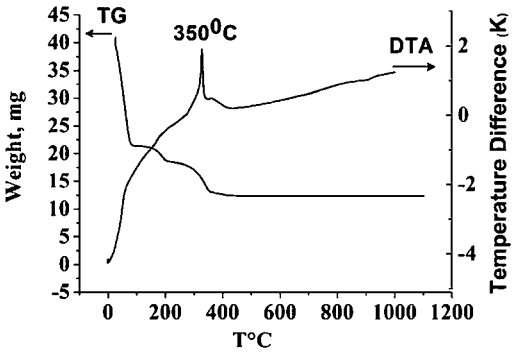

Fig. 4. TG-DTA of $NiFe_2O_4$ suspension.

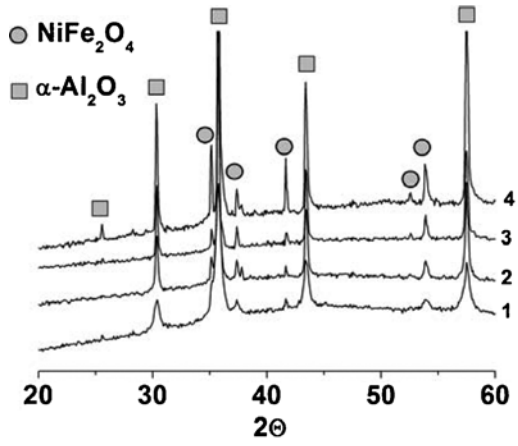

Fig. 6. X-ray diffractions of $NiFe_2O_4$ thick films, obtained at different temperatures: 1, 800 °C; 2, 900 °C; 3, 1000 °C; 4, 1100 °C.

curve is characterized by an exothermic process with a maximum at T = 350 °C. The mass loss of the sample at low temperatures (T = 25–200 °C) is primarily due to removal of adsorbed (H_2O molecules) water and organic solvents with a low boiling point (<200 °C) such as isopropanol and acetylacetone. The mass loss of the sample in the T = 300–450 °C temperature range corresponds to a decomposition of the residual organic components.

Based on these results, the temperature range for the pre-heat treatment of the ferrite films was established at T = 450–500 °C.

Fig. 5 shows the microstructure of the $NiFe_2O_4$ film surface at T = 1000°C obtained using dibutyl phosphate (Fig. 5a) and a mixture of dibutyl phosphate and tannin (Fig. 5b) as dispersants. As follows from Fig. 5b, the film is characterized by more dense surface. This confirms that tannin increases the thick film density.

According to [29], the annealing of the thick films at thermal shock conditions reduces microcracks and pores in the film. Fig. 5c shows the micrograph of the $NiFe_2O_4$ film obtained using a mixture of dibutyl phosphate and tannin as dispersant. The prebaking of thick films was carried out at thermal shock conditions at 500 °C. As follows from Fig. 5c, this film is characterized by high dense surface without microcracks and pores. In this regard, the further prebaking of ferrite spinel $NiFe_2O_4$ and M-type $BaFe_{12}O_{19}$ thick films was carried out at these conditions.

Fig. 6 shows the diffraction patterns of the $NiFe_2O_4$ films obtained in the T = 800–1100 °C temperature range. All samples are single-phase $NiFe_2O_4$. The films obtained at T = 800–1100 °C are characterized by higher adhesion to the substrate. The investigation of the thick films microstructure shows that it is characterized by thickness of ~30 μm (Fig. 7a) and plate-like grains (D_{AV} = 1.5 μm) (Fig. 7b).

3.2. M-type barium ferrite $BaFe_{12}O_{19}$

The monodisperse weakly-agglomerated nanoparticles with an average diameter D_{AV} = 60 nm were used for the synthesis of the M-type $BaFe_{12}O_{19}$ thick films (Fig. 8). Average particles sizes obtained from results of tem are consistent with the particles sizes, calculated from the broadening of X-ray reflections ($D_{AV.}$ = 60 nm).

Fig. 9 shows the diffraction patterns of M-type $BaFe_{12}O_{19}$ films obtained in the T = 1000–1300 °C temperature range. As follows from Fig. 9, the films obtained in the T = 1000–1200 °C temperature range are single-phase. With increasing annealing temperature of the films to 1300 °C we observed the presence of only α-Fe_2O_3 phase on the diffraction pattern. This can be explained by the mutual diffusion of substrate and film components, as indicated by the results of EDX-analysis (Fig. 10). As follows from Fig. 10, the film is characterized by non-uniform elemental composition. The upper surface layer of the film is characterized by the presence of iron, oxygen and a small percentage (2.28%) of aluminium which diffuses into the film. Closer to the film-substrate boundary concentration of iron decreases (from 70% to 13.41%) and its small portion diffuses into the substrate. At the same time, the increasing of the film annealing temperature to 1300 °C contributes to a segregation of barium on the film–substrate interface. The presence of the α-Fe_2O_3 phase between substrate and barium hexaferrite film could have a negative effect on composite structure microwave properties, owing to subsidiary wideband magnetic losses; thus, only film with minimum iron-oxide content was taken for RF measurements.

The $BaFe_{12}O_{19}$ films obtained at T = 1200 °C are characterized by the higher adhesion to the substrate. The investigation of the $BaFe_{12}O_{19}$ thick films microstructure shows that it has a ~50 μm thickness (Fig. 11a) and plate-like grains (D_{AV} = 800 nm) (Fig. 11b).

3.3. Investigation of the high-frequency properties of heterostructures with spinel $NiFe_2O_4$ and M-type $BaFe_{12}O_{19}$-thick films

Transmission characteristics of alumina–nickel ferrite resonator, excited on the main quasi-$H_{01\delta}$ mode are shown in Fig. 12.

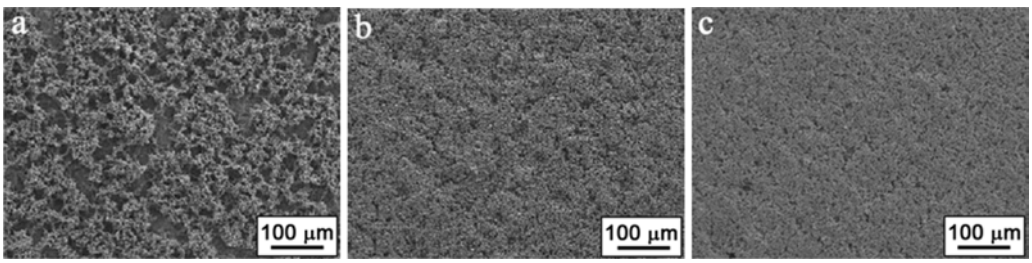

Fig. 5. The microstructure of the surface of the $NiFe_2O_4$ film at T = 1000 °C (SEM) using dibutyl phosphate (a) and a mixture of dibutyl phosphate and tannin (b) as dispersants. (a and b) Slow heating rate; (c) thermal-shock conditions.

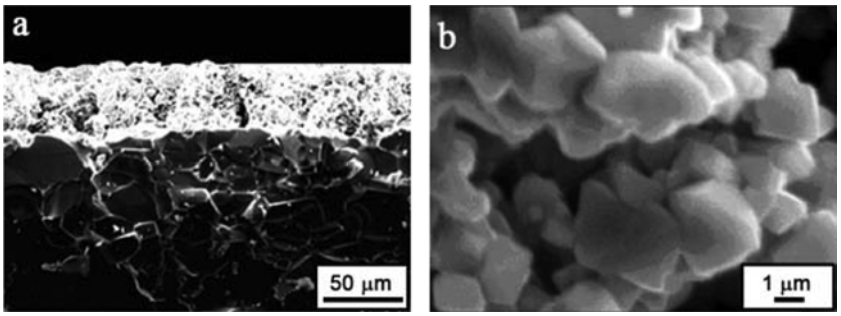

Fig. 7. The microstructure of the cross-section (a) and surface (b) of the $NiFe_2O_4$ film at $T = 1100\,^{\circ}C$ (SEM).

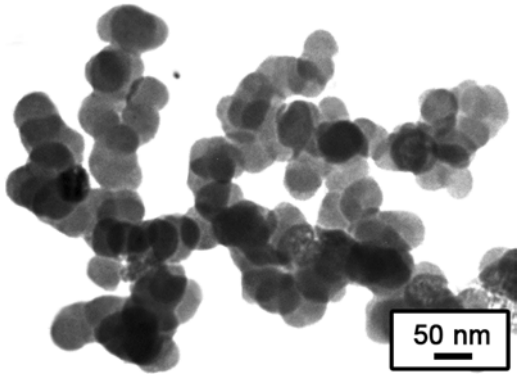

Fig. 8. The microstructure of M-type $BaFe_{12}O_{19}$ nanoparticles, obtained at $T = 1000\,^{\circ}C$.

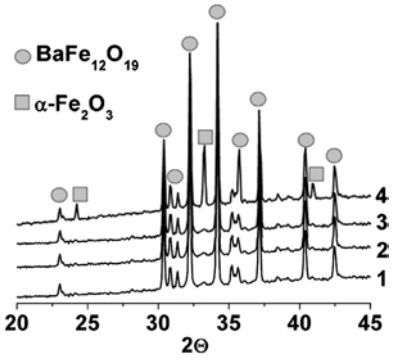

Fig. 9. X-ray diffractions of M-type $BaFe_{12}O_{19}$ thick films, obtained at different temperatures: 1, 1000 °C; 2, 1100 °C; 3, 1200 °C; 4, 1300 °C.

When magnetic field was applied, peak absorption level monotonically decreased (starting form approx. 1 kOe), reached minimum at some specific value of H_0 (compare solid and dash–dotted curves in Fig. 12), and then increased, approaching in large fields its initial value. The magnitude of the absorption level change was found to be 4 dB. Simultaneously, an insignificant variation of resonance frequency (less than 10 MHz) was observed.

Transmission characteristics of α-Al_2O_3–barium hexaferrite composite resonator, excited on one of the higher order dielectric modes (we identified it as $E_{23\delta}$) for different magnitudes of bias magnetic field are shown in Fig. 13. All of the observed dielectric modes reacted on applied magnetic field in various degrees (the drop of S_{21} at high-frequency side of Fig. 13 is just caused by one of those dielectric modes, with weaker absorption and marginal reaction on magnetic field), and here we present only the most prominent result. In general, regardless of the drastically different operating frequency, the observed picture is similar to that in the nickel ferrite case. Maximum change of the peak absorption level amounted to 6 dB, whereas resonance frequency shift did not exceed 30 MHz. However, in this case, absorption level decreasing began from much larger value of bias field, namely $H_0 \approx 7000$ Oe. Such difference between $NiFe_2O_4$ and $BaFe_{12}O_{19}$ is codetermined by the two following reasons: (1) saturation magnetization of

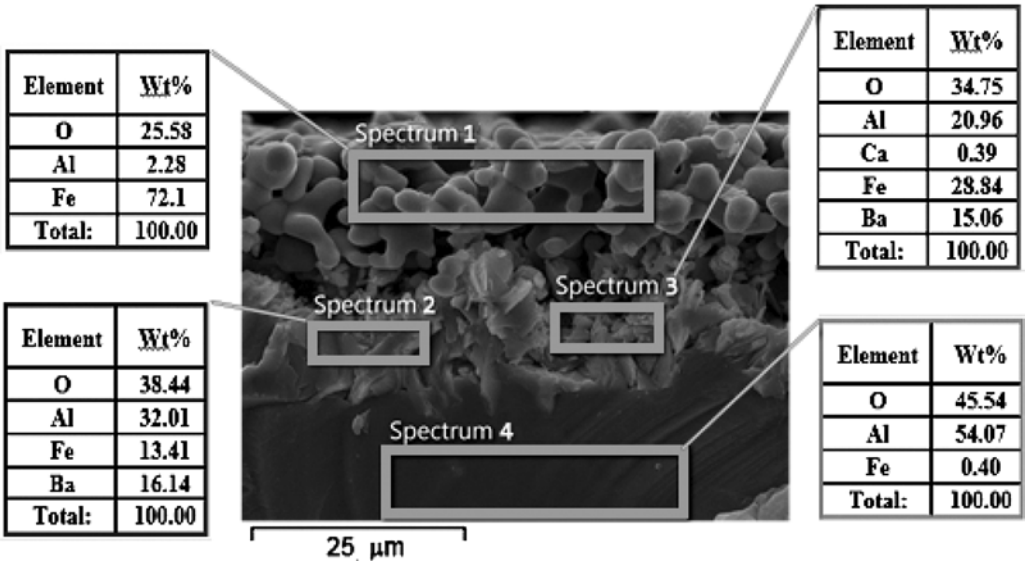

Fig. 10. Distribution of iron and barium ions on the $BaFe_{12}O_{19}$ film surface after heat treatment at $T = 1300\,^{\circ}C$ (EDX).

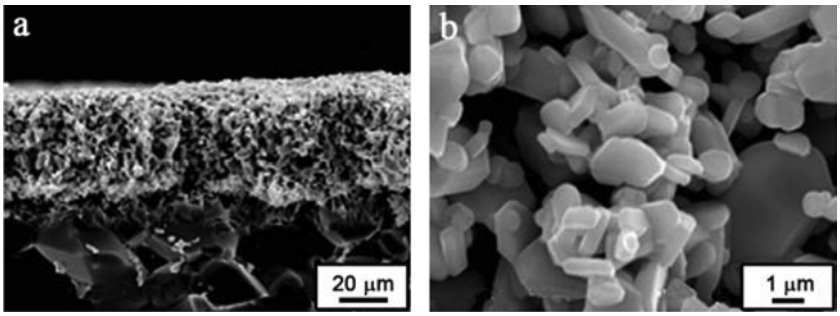

Fig. 11. The microstructure of the cross-section (a) and surface (b) of the $BaFe_{12}O_{19}$ film at $T = 1200\,^{\circ}C$ (SEM).

barium hexaferrite is higher and, hence, field required for sample saturation is also higher; (2) frequency interval between natural domain resonance frequency and corresponding dielectric mode is drastically different (≈10 GHz for the nickel ferrite and ≈24 GHz for the barium hexaferrite).

Because of the limited magnitude of magnetic field, created by electromagnet, we could not track the restoration of zero-field absorption level at large H_0, however the tendency was exactly the same as for the nickel ferrite.

Electrodynamic properties of ferrite layer are determined by the high-frequency magnetic permeability tensor. Its transversal diagonal components for the case of ferro-dielectric with magnetic losses have the form [30]:

$$\mu = \mu' - i\mu'' = \frac{\omega^2 - (\omega_H + i\Delta H/2)(\omega_H + i\Delta H/2 + \omega_M)}{\omega^2 - (\omega_H + i\Delta H/2)^2} \quad (1)$$

where $\omega_H = \gamma H_i$, $\omega_M = \gamma 4\pi M$, H_i the internal magnetic field, including external bias field H_0, dipole–dipole demagnetizing field and anisotropy field (cubic for nickel ferrite and uniaxial for barium hexaferrite), $4\pi M$ the saturation magnetization, $\gamma = \gamma = 2\pi \times 2.8 \times 10^6$ Oe s^{-1} the gyromagnetic ratio and ΔH is the FMR linewidth.

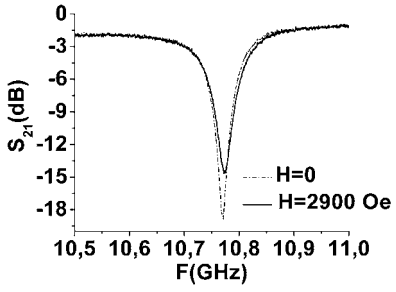

Fig. 12. Modification of the nickel ferrite-dielectric resonator transmission characteristic with applied external magnetic field.

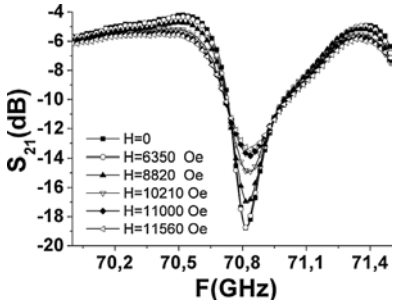

Fig. 13. Transmission characteristics of barium hexaferrite-dielectric resonator at different values of bias magnetic field.

Typical example of μ' and μ'' near-FMR frequency dependence for the case of nickel ferrite is shown in Fig. 14.

Taking into account, that in heterostructure under consideration the volume of ferrite film is much smaller than that of dielectric, we can apply the results of perturbation theory, assuming that dielectric resonator of volume V itself is an unperturbed system and deposited ferrite layer with $\Delta V \ll V$ is a perturbation [31]. We imply that ferrite does not disturb the spatial distribution of the electromagnetic field of DR specific mode. Then, neglecting gyrotropic properties of ferrite, we can approximately calculate the change in DR mode eigenfrequency due to addition of the ferrite [31]:

$$\frac{|\Delta F_r|}{F_r}(H_0) \approx \frac{1}{2}(\mu'(H_0) - 1)\frac{\Delta V}{V} \quad (2)$$

Here, we included only contribution from magnetic permeability, since frequency shift due to difference in dielectric constants does not depend on magnetic field. Using (1) and (2), we can evaluate the effect of magnetic field on resonator frequency. Thus, assuming $\Delta H = 1000$ Oe (such large value of FMR linewidth can be explained by poor morphology of the film and random orientation of the crystallites with respect to the bias field) from (1) we get $(\mu')_{max} \approx 3$ and using $\Delta V/V = 0.001$, we obtain $\Delta F_r \approx 11$ MHz, that is of one order of magnitude with experimental values.

The frequency shift is proportional to the product of relative change of real part of magnetic permeability and ferrite film fractional volume, which is rather small value, therefore resulting ΔF_r is negligible. However, this is not the case for Q-factor. Indeed, we have $\Delta(1/Q_0)(H_0) \approx \mu''(H_0)(\Delta V/V)$ [31]. If one re-writes this expression as $\Delta Q_0/Q_0(H_0) \approx -Q_0\mu''(H_0)(\Delta V/V)$, it becomes clear, that Q-factor fractional change is, in essence, Q_0 times enhanced in comparison with fractional change of resonant frequency, see (2). Thus, even small quantity in right-hand side of the above equation, being Q_0 times magnified, can lead to drastic changes in unloaded Q-factor, and, consequently, composite resonator transmission characteristic. In principle, perturbation theory allows to estimate the change in the unloaded quality factor. However our

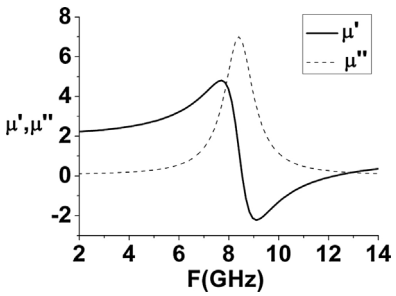

Fig. 14. $\mu'(F)$ and $\mu''(F)$ at frequencies near FMR for nickel ferrite, calculated assuming $4\pi M$ = 3500 G, H_i = 3000 Oe, ΔH = 500 Oe.

calculation revealed more than 50% discrepancy with experiment. This means, that for Q-factor evaluation one need to use full expressions from perturbation theory, without resorting to simplifying approximations. However, this requires knowledge of actual electromagnetic field distribution inside composite resonator, which is unavailable.

The existing models of electrodynamic resonator in transmission line allow us to explain the evolution of resonance absorption line shape both qualitatively and quantitatively. According to [4], linear transmission at resonance frequency is given by $T = 1/(1 + K)$, where coupling coefficient K depends on the specific type of transmission line, shape and size of the resonator, its dielectric constant, resonance wavelength and is proportional to the resonator unloaded Q-factor. In turn, in the case of a composite resonator unloaded Q-factor is inversely proportional to the total losses in bulk dielectric and in ferrite film. Hence, at FMR resonance field, when μ'' reaches maximum, we have increase of losses and decrease of Q_0. Consequently, coefficient K also decreases, leading to overall reduction of transmission losses at composite resonator resonance frequency.

From the data, presented in Fig. 12, we calculated, that $K(H_0 = 0)/K(H_0 = 2900)$ is equal to 1.72 ± 0.04, while unloaded Q-factors ratio is $Q_0(H_0 = 0)/Q_0(H_0 = 2900) = 1.79 \pm 0.12$. Therefore model prediction, that $K \propto Q_0$ [4] indeed holds true. This proves that change in composite resonator transmission characteristic is explained by the degradation of heterostructure unloaded Q-factor due to increased losses in magnetic component at frequencies near FMR.

4. Conclusions

Requisite organic suspensions for thick high-density high-quality $NiFe_2O_4$ spinel and M-type barium hexaferrite ($BaFe_{12}O_{19}$) films synthesis were developed. Using these suspensions, a 30 μm $NiFe_2O_4$ and 50 μm $BaFe_{12}O_{19}$ films were deposited on the surface of an α-Al_2O_3 dielectric resonator by tape-casting. It was found, that microstructure of nickel ferrite and barium hexaferrite was characterized with lamellar grains with average diameter $D_{AV.} = 1.5$ μm and 300 nm, respectively. The temperature range for the pre-heat treatment of the films and its annealing conditions have been defined (T = 450–500 °C, thermal-shock conditions).

A research on possibility of the electronic control of composite "α-Al_2O_3 dielectric resonator-thick ferrite film" structures high-frequency properties has been conducted. Resonance absorption characteristics of such heterostructure with and without applied bias magnetic field were recorded and analyzed. It was found, that magnetic field induces negligible shift of resonance frequency while drastically alter unloaded Q-factor and transmission characteristic of composite resonator. Specifically, change of peak absorption value amounted from 4 to 6 dB.

Worth to note, that qualitatively similar results were obtained for both cm-wave (in this case ferrite component was nickel ferrite) and mm-wave resonators (made using barium hexaferrite film), hence suggested here technique for electronic control over dielectric resonator properties can be successfully utilized in a very broad frequency range, spanning from 1 to 100 GHz, just by selecting the proper ferrite constituent.

It was shown, that changes in heterostructures transmission properties were completely conditioned by increase of magnetic part of the composite resonator internal losses. Estimation of the frequency shift, using perturbation theory, have shown a satisfactory agreement with experiment, which was not the case for the Q-factor, implying that full (and not approximate) expressions should be used during calculations of heterostructure relaxation characteristics.

From our experimental investigations and theoretical estimations, we infer that in order to increase the observed effect (in terms of both frequency shift and Q-factor tuning) we need to further improve thick film deposition technique, with the aim to get as small ferrite FMR linewidth as possible. As far as a ferrite film thickness of 100–200 μm is required in order to get low microwave magnetic losses [17], our next task would be to deposit and investigate such thicker films.

Appendix A. Supplementary data

Supplementary data associated with this article can be found, in the online version, at http://dx.doi.org/10.1016/j.mseb.2015.03.008.

References

[1] J.D. Adam, L.E. Davis, G.F. Dionne, E.F. Schloemann, S.N. Stitzer, IEEE Trans. MTT 50 (2002) 721–737.
[2] D.R. Vizard, Microwave J. 49 (2006) 22–36.
[3] V.G. Harris, Z. Chen, Y. Chen, S. Yoon, T. Sakai, A. Gieler, et al., J. Appl. Phys. 99 (2006), 08M911-1-08M911-5.
[4] M.E. Ilchenko, E.V. Kudinov, Ferrite and Dielectric Microwave Resonators, Kyiv University Publisher, Kyiv, 1973 (in Russian).
[5] D. Kajfez, P. Guillon, Dielectric Resonators, 2nd ed., Noble Publishing Corporation, Atlanta, 1998, pp. 547.
[6] C. Wang, A. Zaki Kawthar, IEEE Microwave Mag. 8 (2007) 115–127.
[7] I.M. Bezborodov, T.N. Narytnik, V.B. Fedorov, Filtry SVCh Na Dielektricheskikh Rezonatorakh. Tekhnika, Kiev, 1989 (in Russian).
[8] I.S. Kovalev, Design and Calculation of Stripline Devices (in Russian), Sovetskoe Radio, Moscow, 1974.
[9] O.G. Vendik, E.K. Hollmann, A.B. Kozyrev, A.M. Prudan, J. Supercond. 12 (1999) 325–338.
[10] R.R. Mansour, IEEE Microwave Mag. 10 (2009) 84–98.
[11] J. Krupka, A. Abramowicz, K. Derzakowski, IEEE Trans. Microwave Theory Tech. 54 (2006) 2329–3335.
[12] Y.M. Poplavko, Y.V. Prokopenko, V.I. Molchanov, A. Dogan, IEEE Trans. MTT 49 (2001) 1020–1026.
[13] T. Plutenko, O. V'yunov, Solid State Phenomena 200 (2013) 311–315.
[14] G.L. Turin, IEEE Trans. Inform. Theory 6 (1960) 311–329.
[15] A.H. Gholamipour, A. Gorcin, H. Celebi, B.U. Toreyin, M.A.R. Saghir, F. Kurdahi, A. Eltawil, Reconfigurable filter implementation of a matched-filter based spectrum sensor for cognitive radio systems, IEEE International Symposium on Circuits and Systems (ISCAS), 2011, pp. 2457–2460.
[16] M.A. Popov, I.V. Zavislyak, G. Srinivasan, Magnetic field controlled nonreciprocal band-stop filters for the w-band using magnetic polariton modes in yttrium-iron garnet, Progress in Electromagnetics Research Symposium Abstracts, Stockholm, Sweden, 2013, p. 32.
[17] V.G. Harris, IEEE Trans. Mag. 48 (2012) 1075–1104.
[18] V.G. Harris, A. Geiler, Y. Chen, S.D. Yoon, M. Wu, A. Yang, Z. Chen, P. He, P.V. Parimi, X. Zuo, C.E. Patton, M. Abe, O. Acher, C. Vittoria, J. Magn. Magn. Mater. 321 (2009) 2035–2047.
[19] C. Barry Carter, M. Grant Norton, Ceramic Materials: Science and Engineering, Springer. Science & Business Media, 2013, pp. 799.
[20] S. Courreges, Z. Zhao, K. Choi, A. Hunt, J. Papapolymerou, In Tech Open (2010) 185–204 (chapter 8).
[21] O.V. Yelenich, S.O. Solopan, T.V. Kolodiazhnyi, V.V. Dzyublyuk, A.I. Tovstolytkin, A.G. Belous, Solid State Sci. 20 (2013) 115–119.
[22] E.V. Pashkova, E.D. Solovyova, I.E. Kotenko, T.V. Kolodiazhnyi, A.G. Belous, J. Magn. Magn. Mater. 323 (2011) 2497–2503.
[23] D. Peddis, F. Orru, A. Ardu, C. Cannas, A. Musinu, G. Piccaluga, Chem. Mater. 24 (2012) 1062–1071.
[24] D.B. Nicholson, Hewlett-Packard J. 41 (1990) 59–61.
[25] A.K. Maiti, B. Rajender, Mater. Sci. Eng. A 333 (2002) 35–40.
[26] L.A. Salam, R.D. Matthews, J. Eur. Ceram. Soc. 25 (2005) 863–873.
[27] T. Chartier, E. Streicher, P. Booch, Ceram. Bull. 66 (1987) 1653–1655.
[28] L. Shouci, J.P. Robert, E. Forssberg, Interfacial Separation of Particles, Elsevier, Amsterdam, 2005, pp. 706.
[29] B.V.R. Chowdari, J. Kawamura, J. Mizusaki, K. Amezawa, Solid State Ionics: Ionics for Sustainable World, World Scientific, Sendai, Japan, 2012.
[30] A.G. Gurevich, G.A. Melkov, Magnetization Oscillations and Waves, CRC Press, New York, 1996.
[31] L.F. Chen, C.K. Ong, C.P. Neo, V.V. Varadan, V.K. Varadan, Microwave Electronics: Measurement and Materials Characterization, John Wiley & Sons, Ltd., Chichester, England, 2004, pp. 537.